

## Article

# Spreading Behavior of Single Oil Droplet Impacting Surface with/without a Thin Liquid Film

He Liang <sup>1</sup>, Peiyi Yang <sup>1</sup>, Wenzhong Wang <sup>1,\*</sup> , Yanfei Liu <sup>1</sup> , Xiangyu Ge <sup>1</sup>  and Baohong Tong <sup>2</sup><sup>1</sup> School of Mechanical Engineering, Beijing Institute of Technology, Beijing 100081, China<sup>2</sup> School of Mechanical Engineering, Anhui University of Technology, Ma'anshan 243032, China

\* Correspondence: wangwzhong@bit.edu.cn

**Abstract:** When oil droplets impact a solid surface for oil-air lubrication, they may spread out to produce a thin oil layer on the surface, which serves as a significant source of lubrication. A test rig was constructed in this research to observe the spreading behavior of oil droplets impacting surfaces from both frontal and lateral views. From the frontal view, laser-induced fluorescence techniques are used to measure the thickness of the oil layer quantitatively during the spreading of oil droplets. While the lateral view can observe the shape evolution of the droplets. Oil droplet spreading patterns on the sheet with dry surfaces and with different thin liquid film thicknesses were studied, and the effect of viscosity and the thickness of the thin liquid film on spreading radius and spreading thickness is considered. The experimental findings demonstrate that the maximum spreading factor, the spreading central layer thickness, and the apparentness of retraction all increase as viscosity increases. The retraction is obviously impacted by thin liquid films, and the retraction weakens as the thin liquid film thickness increases.

**Keywords:** oil droplets; impact; liquid film; laser-induced fluorescence; film thickness



**Citation:** Liang, H.; Yang, P.; Wang, W.; Liu, Y.; Ge, X.; Tong, B. Spreading Behavior of Single Oil Droplet Impacting Surface with/without a Thin Liquid Film. *Lubricants* **2023**, *11*, 31. <https://doi.org/10.3390/lubricants11010031>

Received: 14 December 2022

Revised: 6 January 2023

Accepted: 8 January 2023

Published: 12 January 2023



**Copyright:** © 2023 by the authors. Licensee MDPI, Basel, Switzerland. This article is an open access article distributed under the terms and conditions of the Creative Commons Attribution (CC BY) license (<https://creativecommons.org/licenses/by/4.0/>).

## 1. Introduction

During recent decades, oil-air lubrication has been commonly utilized for high-speed rolling bearings [1,2]. In oil-air lubrication, the lubricating oil impacts on the solid surface in the form of oil droplets, some of which impact several times, while others are deposited on the surface and spread to produce a liquid layer with thicknesses ranging from a few microns to several hundred microns. As the spreading liquid layer is an important supply for the formation of a lubricating film in the contact zone formed between the rolling elements and raceways, the spreading of the oil droplets into a liquid layer after impacting the surface should be studied.

Worthington [3] is believed to be the first person to have investigated the phenomenon of oil droplets impacting on surfaces in 1876. He tested the effect of milk and mercury droplets on hydrophobically coated glass sheets and found that the droplets shatter at greater impact speeds. Following that, the impact behavior of the droplets was clearly documented by the use of high-speed cameras. Based on their experimental results, Rioboo et al. [4,5] categorized the impact of a single droplet on a solid surface into several phenomena: deposition, splash, rebound, and partial rebound. Bi et al. [6] discovered that the viscosity of the droplet has a significant impact on the droplet spreading behaviors at a given impact velocity. With decreasing viscosity, the spreading factor  $\beta$  ( $\beta = r_t/r_0$ ) and spreading time (the time required to attain the maximum spreading factor) rise, where  $r_t$  is the instantaneous diameter after contact and  $r_0$  is the droplet's original diameter.

The impact and spreading properties of a droplet may alter significantly when a liquid film is present on a solid surface. The dimensionless thickness of the liquid film is commonly described as  $\delta = h_0/(2r_0)$ , where  $h_0$  denotes the liquid film thickness. A thick liquid film or pool of liquid is defined for  $\delta \gg 1$ , however, the definition of a thin liquid

film is somewhat controversial: some define  $\delta < 1$  as a thin liquid film, others define  $\delta < 0.1$  as a thin liquid film [7–10]. Thin liquid films promote splashing, and the size and quantity of splash droplets are proportional to the dimensionless liquid film thickness. When  $0.1 < \delta < 1$ , two modes of splashing are observed experimentally: prompt splashing (secondary droplets are produced while the crown splash is developing) and delayed splashing (separation of secondary droplets from the top edge of the splash only when the crown splash has developed to its maximum extent); when  $1 < \delta < 10$ , the liquid film inhibits both types of splashing [11].

The studies discussed above are largely qualitative findings that concentrate on the critical conditions for splashing following droplet impact. Quantitative measurements of liquid film spreading have received less attention: on the one hand, reproducibility is poor when the liquid film is thin; on the other hand, there is a lack of quantitative measurement methods, with most researchers relying on direct observation, magnification, or light reflection through laser beams [12,13]. However, most studies are still limited to thick liquid layers [14,15].

In this research, a custom-made test rig was developed to study the spreading behavior of oil droplets impacting surfaces from both frontal and lateral orientations. The frontal observation used laser-induced fluorescence techniques to quantify micron-level oil layer thickness during spreading. Using this approach, the spreading behavior of oil droplets on thin liquid films was studied.

## 2. Experimental

The custom-made test rig consists of an oil drop-generating device, an optical system, a high-speed camera, and a computer, as shown in Figure 1. Oil droplets with a radius of approximately 1.5 mm are generated by the syringe pump. The syringe pump is located on a stage, and oil droplets are free to fall from a specified height and impact a glass sheet with a velocity of  $v = 2.73$  m/s. As oil-air lubrication is usually used in high-speed situations, which can reach up to 10,000 r/min and the impacting speed of the oil droplets can reach a few meters per second, therefore, we use a high impact speed to reproduce the high-speed condition [16]. The Reynolds numbers are calculated as 0.94, 0.23, and 0.079, respectively, for the chosen conditions.

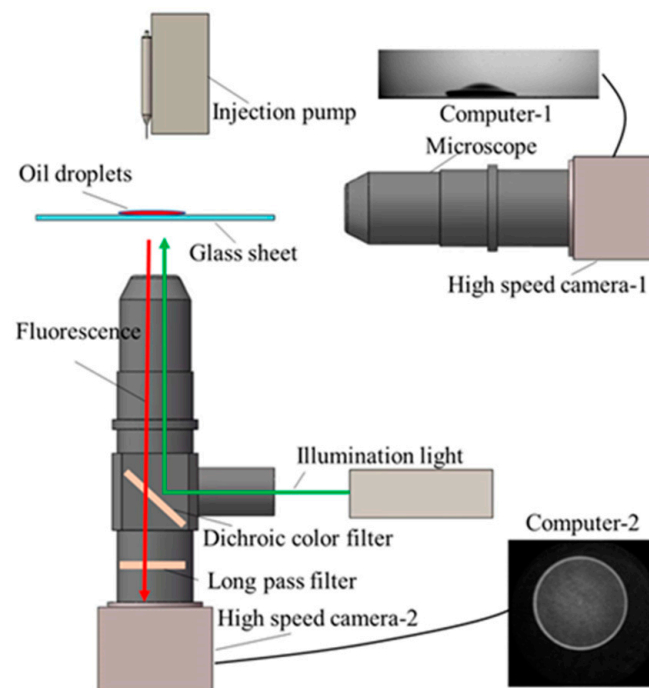


**Figure 1.** Test rig for the impact observation.

The glass sheet is also employed as an optical viewing window. In this research, two optical systems were utilized concurrently. One is for lateral observation, consisting of a high-speed camera (Photron, Japan), an LED light source, and a microscope. The other set is for frontal observation and is placed beneath the glass sheet, which includes a high-speed camera, a laser light source (532 nm), a homogenizer, and a fluorescence microscope. The latter system can measure the thickness of the spreading oil layer based on laser-induced fluorescence techniques.

The glass sheet is cleaned before each test. As the stains on the used glass sheet are mainly dust and lubricating oil, the glass sheet is first cleaned with alcohol to remove most of the lubricating oil, then with detergent to clean the lubricating oil and alcohol, and next with a large amount of water before finally being wiped and dried.

By measuring the fluorescence intensity, the laser-induced fluorescence approach can assess the thickness and distribution of the oil layer based on the Beer–Lambert law [17], which describes the relationship between the thickness of the oil layer per unit area and the fluorescence emitted as a specified exponential relationship:

$$I_f(h) = kI_0\Phi\{1 - \exp[-\varepsilon(\lambda_{\text{laser}})Ch]\} \quad (1)$$

where  $I_f(h)$  is the fluorescence captured by the camera,  $I_0$  is the illumination light with homogeneous distribution and constant intensity,  $\Phi$  is the quantum efficiency,  $k$  is the monitoring efficiency of the camera,  $\varepsilon(\lambda_{\text{laser}})$  is the molar absorptivity,  $C$  is the molar concentration of the fluorescent dye in the fluid, and  $h$  is the thickness of the fluid film.

As, in practice, the fluorescence emission by the oil is weak, a fluorescent dye can be evenly dissolved in the lubricant to enhance its excited fluorescence intensity. The fluorescent dye used in the experiments is pyromethene, which is non-toxic, physiochemically stable, and soluble. Due to the exponential function, optimizing  $\varepsilon(\lambda_{\text{laser}})C$  can significantly improve the measurement range and accuracy, according to Equation (1). Once the fluorescent dye is selected,  $\varepsilon(\lambda_{\text{laser}})$  is a constant value, and the concentration of fluorescent dye  $C$  can be optimized. The concentration of fluorescent dye is chosen to be 1.5 mmol/L in the present study.

In the experiment, the image captured by the high-speed camera is a grey-scale graph, which is used to represent fluorescence intensity. Equation (1) is simplified as follows:

$$h = \frac{1}{B}(\ln A - \ln(A - I)) + C \quad (2)$$

where  $I$  is the grey scale value,  $A$ ,  $B$ , and  $C$  are constants, and  $C$  is the correction parameter.

Prior to the experiment, calibration is necessary to get a quantifiable relationship between the thickness of the oil layer and the grayscale value. Figure 2 shows the calibrating procedure. Taking oil PAO4 as an example, a steel ball with a radius  $r = 3.97$  mm is placed on the optical glass sheet, and the oil tagged with fluorescent dye fills the gap formed between the ball and the glass sheet. The geometric relation can be used to calculate the clearance of the gap between the steel ball and the glass sheet at any location (Figure 2b). The fluorescence intensity emitted by the oil film at the corresponding location is obtained by the camera and expressed as a grayscale value (Figure 2c). The larger the gap, the larger the corresponding grey scale value. The fitting curve between the oil thickness value and the grayscale value is illustrated in Figure 2d and by Equation (3).

$$h = \frac{1}{0.00382}(\ln(43.68135) - \ln(43.68135 - I)) - 11 \quad (3)$$

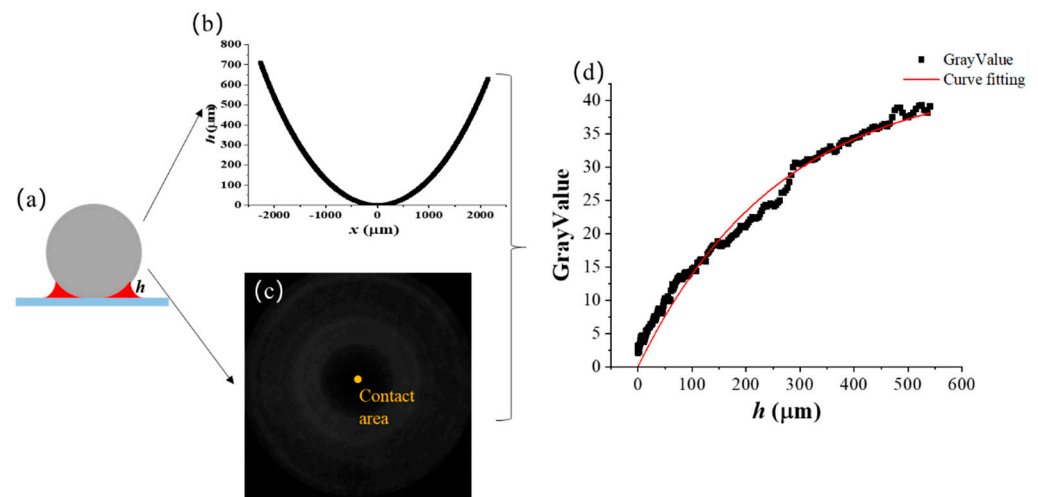


**Figure 2.** Calibration between oil layer thickness and fluorescence intensity: (a) Steel ball was placed on a glass sheet with sufficient oil supply; (b) Calculated gap between steel ball and glass sheet; (c) Grey value picture of oil layer; (d) Relationship between oil layer thickness and grayscale value.

Table 1 shows the physicochemical parameters of the three synthetic base oils used in the tests. Polyalphaolefin oil has been widely used and is a Newtonian fluid [18]. The lubricant viscosity is measured using a Modular Compact Rheometer (MCR 302), and the surface tension and contact angle are determined using a Data-Physics Instruments (ESr-N). When measuring the contact angle, a small droplet generated by the syringe pump (volume of 3  $\mu\text{L}$ ) is softly sited on the glass sheet. As the contact angle decreases with time, the data in this paper is collected after five seconds of spreading. For each sample, three replicas (randomly located on the surface) are performed for all batches. All parameters were measured at room temperature ( $t = 25 \pm 1$   $^{\circ}\text{C}$ ). A high-speed camera operating at a frame rate of 6400 fps and an exposure length of 1/6400 s is utilized to record the spreading of the oil droplets following impact with the surface.

**Table 1.** Oil parameters.

Category	Density ( $\text{kg}\cdot\text{m}^{-3}$ )	Viscosity (25 $^{\circ}\text{C}$ ) (mPa·s)	Surface Tension ( $\text{mN}\cdot\text{m}^{-1}$ )	Contact Angle ( $^{\circ}$ )
PAO2	0.7988	6.962	24.254	8.7
PAO4	0.819	29.59	28.765	16.9
PAO8	0.8326	86.545	29.356	17.2

### 3. Experimental Results

#### 3.1. Spreading Behavior of Oil Droplets Impacting a Dry Surface

Three different oils, PAO2, PAO4, and PAO8, in droplet form, are chosen to impact the dry surface. Typical photos captured from the lateral side are shown in Figure 3. The initial impact velocity is  $v = 2.73$  m/s, the droplet's initial radius is  $r_0 = 1.5$  mm, and the droplet begins to touch the surface at  $t = 0$  ms. The Weber numbers ( $We = 2\rho v^2 r_0 / \sigma$ ) for the three oils are calculated to be 0.74, 0.64, and 0.63, respectively, and the Capillary numbers ( $Ca = \mu v / \sigma$ ) are calculated to be 0.78, 2.81, and 8.05, respectively. As the surface tension and density of the chosen oils are quite close, the Weber numbers for the oils are similar. The difference in the Capillary number for the oils is mainly caused by viscosity. Therefore, when the impact speed is fixed, the droplet pattern dynamics are dependent on the oil viscosity for the same type of oil.

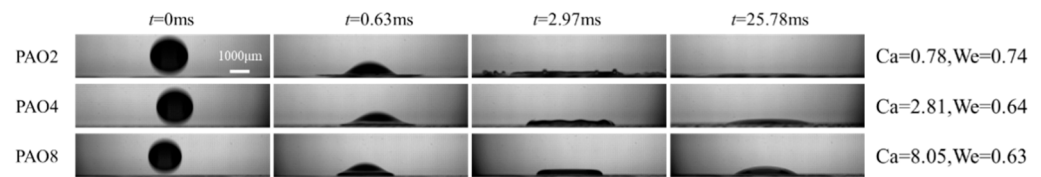


**Figure 3.** Comparison of the morphology of different oil droplets impacting the dry surface from lateral view ( $v = 2.73$  m/s,  $r_0 = 1.5$  mm).

The PAO2 droplet can remain spherical until it impacts the dry surface ( $t = 0$  ms), after which it collapses quickly and spreads out, creating a hat shape at  $t = 0.63$  ms. At  $t = 2.97$  ms, the droplet continues to spread, increasing the spreading radius  $r_t$  and decreasing the layer thickness in the central area. At  $t = 25.78$  ms, the spreading radius achieves a stable state as a thin film layer. PAO4 and PAO8 spread like PAO2. At  $t = 0.63$  ms, the spherical droplets collapse and spread into a hat form. At  $t = 2.97$  ms, irregular tiny droplets develop at the periphery of the PAO4 droplets but remain linked with the main body; the PAO8 droplet spreads in a pie shape and no splattered droplets are observed. At  $t = 25.78$  ms, both the PAO4 and PAO8 droplets retract: the layer thickness drops in the edge area, while it rises in the central area, resulting in the shape of a spherical crown.

The lateral view shows the morphological changes for the impact and spreading of the oil droplets. The oil layer thickness, however, can hardly be measured. Therefore, the laser-induced fluorescence technique is used to measure the thickness of the oil layer from the frontal view.

Figure 4 shows frontal grayscale photographs of three different oil droplets impacting dry surfaces utilizing a laser-induced fluorescence technique. According to the laser-induced fluorescence principle mentioned in the preceding section, a larger grayscale value stands for thicker oil layer thickness. Due to the limitation of the thickness measurement range of the fluorescence method, the thickness of the oil layer at the beginning stage is too large to be quantified, therefore only the distribution of oil layers with a thickness of fewer than  $500 \mu\text{m}$  is of interest. Defining the spreading center as the origin, the oil droplet is basically symmetrically disseminated from the center. When the spreading radius  $r_t$  is beyond the observation range, half of the distribution can be focused on (as shown in Figure 4b). At  $t = 0.94$  ms, the central area of the PAO2 spreading layer is brighter, implying a thicker oil layer, while the edge region is darker, indicating a thinner oil layer. The edge of the oil layer has a regular distribution of bright spots (Figure 4a), which should be the splash of oil droplets (daughter droplets), in contrast with Figure 3. The daughter droplets originate from the edge area of the droplet during impact. In the process of spread, part of the energy is gathered in the daughter droplets at the edge area, causing them to separate from the edge [11]. At  $t = 2.97$  ms, the spreading radius  $r_t$  increases while the brightness of the oil layer in the central area decreases, indicating that the thickness gradually decreases; at  $t = 5.31$  ms, there is no obvious change in the spreading radius  $r_t$ , and the brightness of the central area does not change significantly, while the brightness near the edge increases, indicating that the layer thickness in the edge increases. At  $t = 25.78$  ms, there is no noticeable change in the spread radius  $r_t$ , the brightness of the center area increases, making the difference between the brightness of the central area and that of the edge area decrease, and retraction can be observed.

The PAO4 and PAO8 oil droplets spread in the same manner as the PAO2 oil droplets. The edges of the PAO4 oil layer show an irregular shape at  $t = 0.94$  ms, whereas the edges of the PAO8 oil layer are more uniform. No splashing is found for either oil. At  $t = 2.97$  ms, the spreading radius  $r_t$  of both oil droplets is smaller than that of PAO2. The spreading radius  $r_t$  of PAO4 is larger than that of PAO8, and the brightness of the central area is weaker, with small oil droplets (daughter droplets) in the edge area. It can be observed that most of the daughter droplets are not separated from the main body and finally return to the main body, while only a few daughter droplets are separated at  $t = 5.31$  ms. The surface tension acts as the resistance force for the deformation of the oil droplet. With

higher surface tension, fewer oil droplets can splash and the daughter droplets can hardly separate from the main body. At  $t = 25.78$  ms, the brightness of the central area of the PAO4 and PAO8 oil layers is greater than that of the edge area, indicating that the central area of the oil layer is thicker than the edge area, and a retraction event occurs.

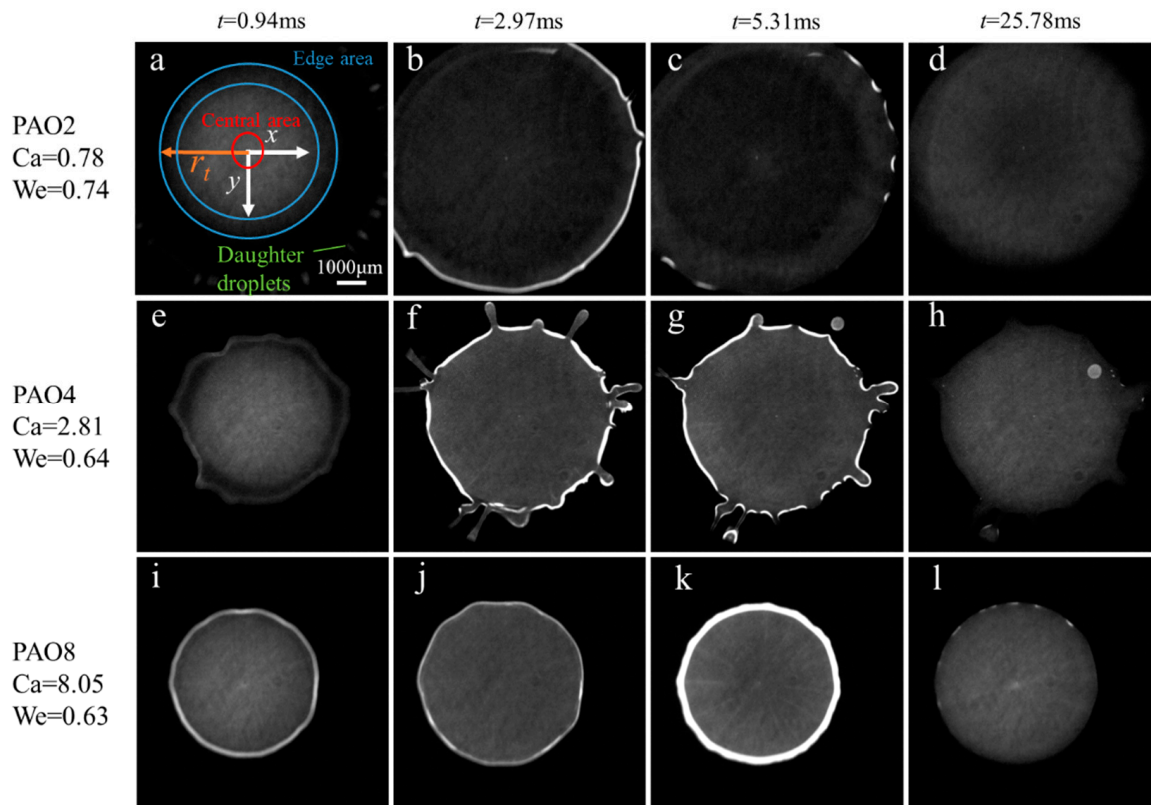


**Figure 4.** Comparison of the frontal view of the morphology of oil droplets impacting a dry surface over time ( $v = 2.73$  m/s,  $r_0 = 1.5$  mm).

The oil layer thickness can be calculated based on Equation (3). Figure 5 depicts the distribution of the cross-sectional oil layer thickness  $h_x$  along the  $x$ -axis during spreading for PAO4. For comparison, a range of  $1000 \mu\text{m}$  from the origin is defined as the central area, and the central layer thickness  $h_z$  is defined as the average of the oil layer thickness in the central area as marked in Figure 4a; a range of  $1000 \mu\text{m}$  from the edge is defined as the edge area, and the edge layer thickness  $h_b$  is defined as the average oil layer thickness. The spreading radius  $r_t$  is about  $3300 \mu\text{m}$  at  $t = 0.94$  ms, the central layer thickness  $h_z$  is much larger than the edge layer thickness  $h_b$ , and the cross-sectional oil thickness distribution is hat-shaped, with a maximum thickness of about  $250 \mu\text{m}$ . At  $t = 2.97$  ms, the spreading radius  $r_t$  grows to be around  $3600 \mu\text{m}$ , the central layer thickness  $h_z$  decreases dramatically while the edge layer thickness  $h_b$  increases and the oil layer shows to be a concave distribution with two higher sides and a lower center, and a bump in the middle. This is compatible with Zheng's modeling results [19] and Chen's experimental results [20]: when droplets collide with the surface, capillary waves arise and propagate along the droplets, causing the deformation of the droplet and an increase in layer thickness near the droplet edge as well as a bulge in the center. At  $t = 16.88$  ms, the spreading radius  $r_t$  remains constant, the central film thickness  $h_z$  grows slightly, while the edge film thickness  $h_b$  falls dramatically; the oil layer thickness distribution resembles a pie shape. The spreading radius remains practically constant from  $t = 2.97$  ms to  $t = 16.88$  ms, with the oil at the edge returning to the central area and retracting. At  $t = 59.06$  ms, the spreading radius  $r_t$  does not change, the central layer thickness  $h_z$  grows, and the edge layer thickness  $h_b$  falls slightly, with a maximum layer thickness of around  $170 \mu\text{m}$ .

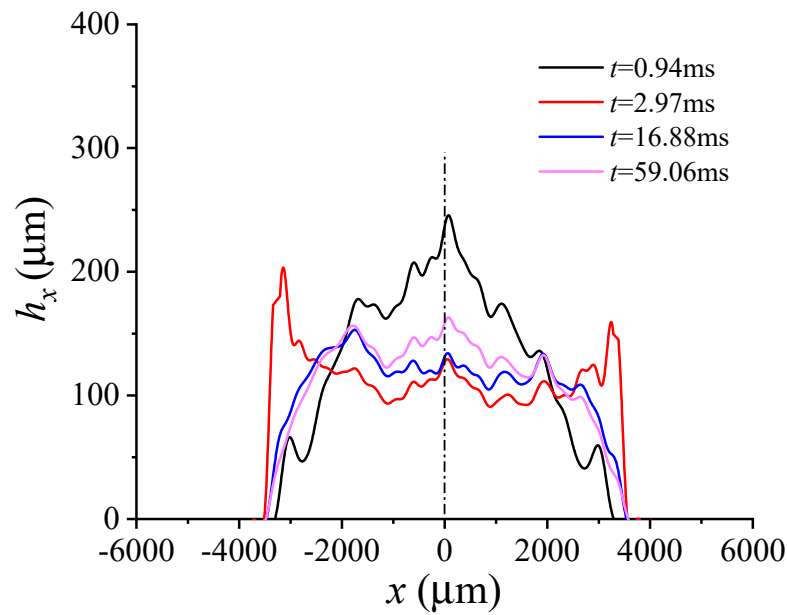


**Figure 5.** Cross-sectional distribution of oil layer thickness along the  $x$ -axis at different moments after PAO4 oil droplets impact on the dry surface ( $v = 2.73$  m/s,  $r_0 = 1.5$  mm).

Figure 6 depicts the comparison of the cross-sectional profiles of oil layer thickness for three oil droplets during the spreading processes. In Figure 6, the PAO8 droplet shows a remarkable coffee-ring-like pattern in time in comparison to other liquids. In fact, this phenomenon exists for all three oils, but it is more evident and lasts for a longer time with higher-viscosity oils. Therefore, it is more clearly found for PAO8 in Figure 6. We speculate that the high spikes at the edges, which show coffee-ring-like patterns, could be caused by the optical distortion at the edge area of the droplet, as, when we compare Figures 3 and 4, there are no high spikes in lateral views (Figure 3). At  $t = 0.94$  ms, the layer thickness distribution of the three droplets remains nearly the same. At  $t = 5.31$  ms, all three droplets spread to produce a thin layer of oil, with a larger viscosity resulting in a smaller spreading radius and a larger central film thickness. The central layer thickness is smaller than the edge layer thickness in all three types of oil droplets, and this tendency becomes pronounced with increasing viscosity. At  $t = 25.78$  ms, all three droplets retract to some extent, resulting in a thicker layer in the central area and a thinner layer at the edges. In addition, a larger viscosity leads to greater retraction.

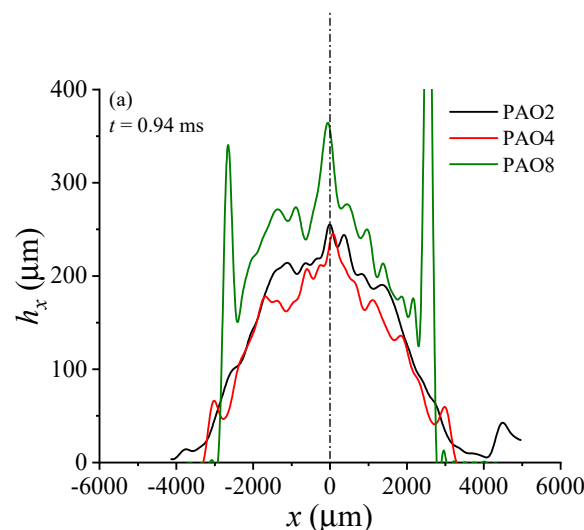


**Figure 6.** Cont.

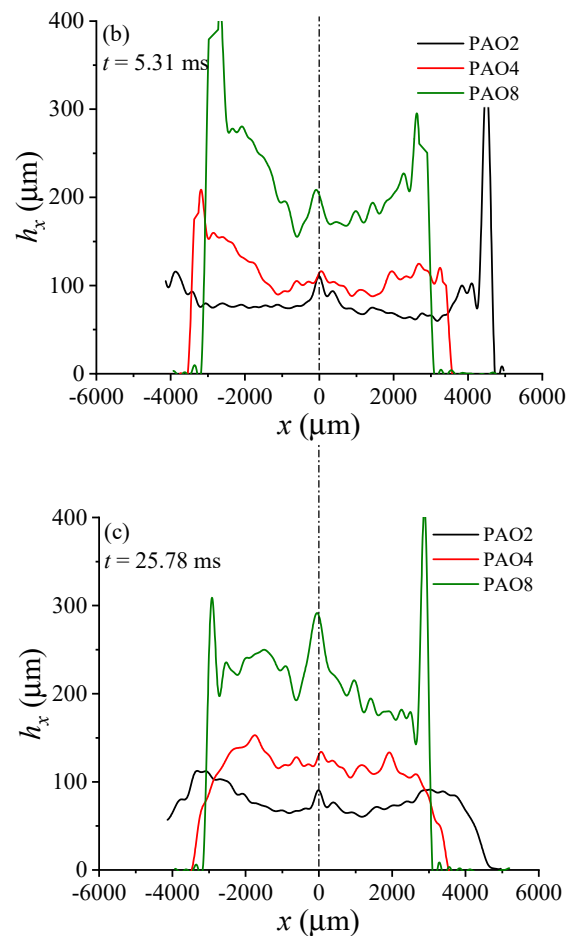


**Figure 6.** Comparison of different oil layer thickness distributions at the same moment ( $v = 2.73$  m/s,  $r_0 = 1.5$  mm): (a)  $t = 0.94$  ms; (b)  $t = 5.31$  ms; (c)  $t = 16.88$  ms.

The spreading radius and central layer thickness of the droplet, which are key boundary conditions for lubrication, are compared independently. Figure 7 depicts the variation in the spreading factor  $\beta$  ( $\beta = r_t/r_0$ ) with time  $t$  after the impact of three droplets on the surface: the spreading factor increases significantly at first and then stabilizes after two to four microseconds. A larger viscosity leads to a smaller spreading factor at the steady state and a smaller rate of change of the spreading factor with time. However, it is quicker to achieve a steady state.

Figure 8 shows the change in the central layer thickness  $h_z$  with time  $t$ . The central layer thickness of PAO2 declines swiftly and then stabilizes, while the central layer thickness  $h_z$  of PAO4 and PAO8 decreases rapidly and then progressively increases after reaching the lowest point. PAO8 takes less time to reach the lowest point, and the following increase in central layer thickness is larger. Corresponding to Figure 7, the spreading radius reaches the maximum and then the central layer thickness reaches its minimum; thereafter, the spreading radius remains stable while the central layer thickness increases primarily due to retraction caused by oil flowing back from the edge to the central area. As Figure 9 shows, the larger the viscosity, the greater the ratio of the central layer thickness to the edge layer thickness, which indicates a more obvious degree of retraction.

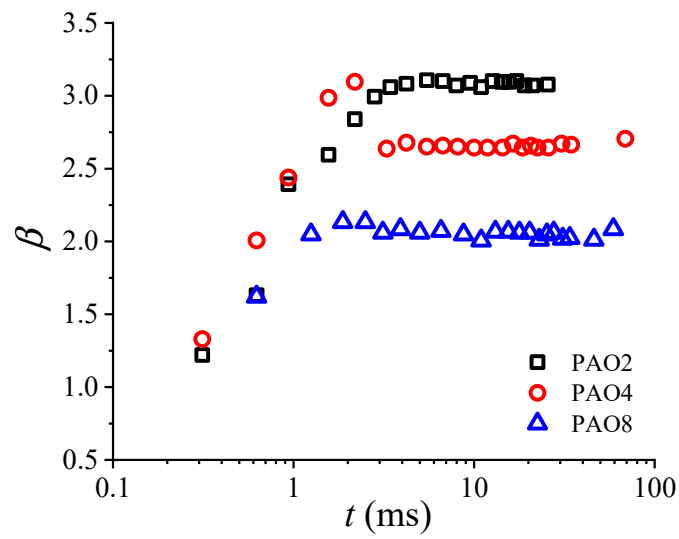


Figure 7. Comparison of different viscosity spreading factors.

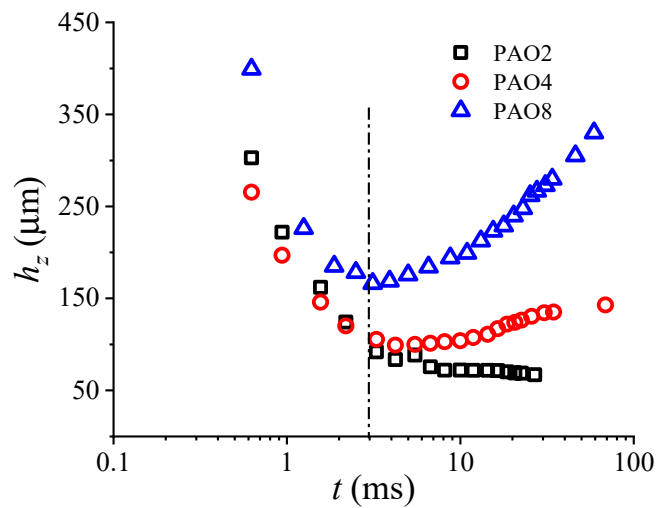


Figure 8. Comparison of the central layer thickness at different viscosities.

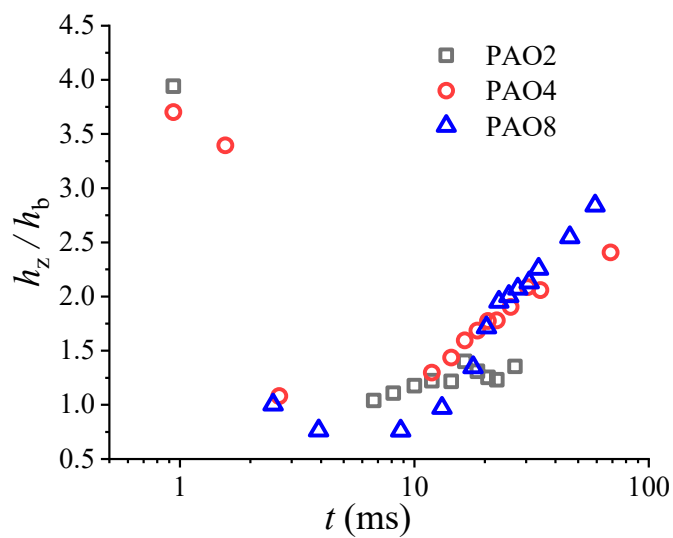
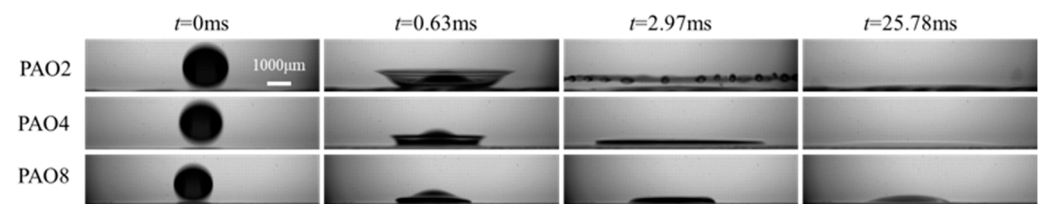


Figure 9. Variation of  $h_z/h_b$  over time for the three oils.

### 3.2. Spreading Behavior of Oil Droplets Impacting the Sheet with Different Thin Liquid Film Thicknesses Thin Liquid Films

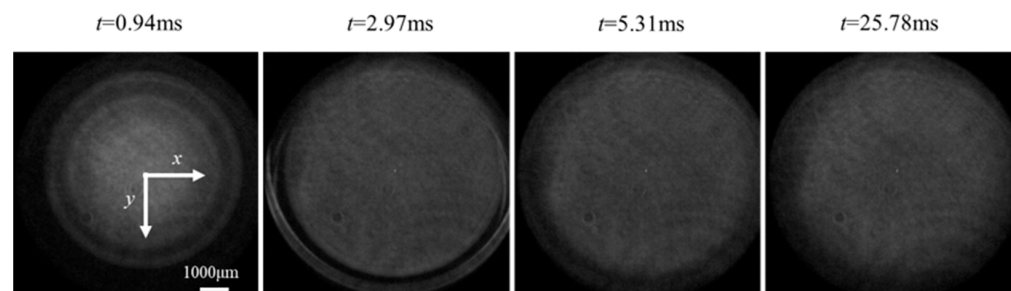
In actuality, the surface cannot be completely dry; generally, it will be covered by a thin liquid film from lubrication during operation. This section studies the spreading phase of oil droplets impacting the sheet with different thin liquid film thicknesses. A homogeneous thin lubricant film is first smeared on the surface of the glass sheet, and the thickness of the liquid film is measured by laser-induced fluorescence. The spreading behavior of the oil droplet impacting the thin liquid film is then studied. The thin liquid film thickness range for this experiment is 0~73  $\mu\text{m}$ , and the dimensionless number varies from 0~0.026.

Figure 10 presents a typical lateral view of the spreading pattern over time for three droplets impacting the sheet with different thin liquid film thicknesses. The droplet's initial impact velocity and radius are kept constant at  $v = 2.73 \text{ m/s}$  and  $r_0 = 1.5 \text{ mm}$ , respectively. When comparing Figure 3 with Figure 10, it is clear that a thin liquid film of even a few tens of microns has a significant effect on the spreading behavior of the oil droplets after the impact on the surface. At  $t = 0.63 \text{ ms}$ , the spreading pattern turns from a hat-shaped to a bowl-shaped splash, and the bowl-shaped splash is also more evident when the viscosity decreases. The spreading radius grows dramatically at  $t = 2.97 \text{ ms}$ , and PAO2 generates a crown-shaped splash, with the splashing droplets separated from the main body. No small droplets are observed at the border of the PAO4 oil layer. The spreading radius achieves a stable state as a thin film layer at  $t = 25.78 \text{ ms}$ , although the thickness of the oil layer is much less than that of the dry surface. The change in droplet impact pattern caused by the thin film is similar to Wang's findings [10]: the thin film increases splashing.



**Figure 10.** Lateral plot comparison of oil droplets impacting the sheet with different thin liquid film thicknesses with time ( $v = 2.73 \text{ m/s}$ ,  $r_0 = 1.5 \text{ mm}$ ).

Figure 11 shows the typical grayscale pictures of a PAO4 oil droplet impacting a sheet with a 33  $\mu\text{m}$  thin liquid film. Oil droplets impacting a thin liquid film spread more evenly, have a larger spreading radius, and take less time to achieve a steady state than droplets impacting on a dry surface.



**Figure 11.** Frontal view of PAO4 oil droplet impacting the sheet with ( $h_0 = 33 \mu\text{m}$ ,  $\delta = 0.011$ ) thin liquid film thickness versus time ( $v = 2.73 \text{ m/s}$ ,  $r_0 = 1.5 \text{ mm}$ ).

Figure 12 shows the cross-sectional profile of oil thickness along the  $x$ -axis at four instants for a PAO4 droplet impacting the sheet with a thin liquid film of 33  $\mu\text{m}$  ( $\delta = 0.011$ ). The spreading radius  $r_t$  is roughly 4900  $\mu\text{m}$  at  $t = 0.94 \text{ ms}$ , which is larger than the spreading radius for oil droplets impacting the sheet with a dry surface. The spreading radius  $r_t$  does not change appreciably at  $t = 1.88 \text{ ms}$ , but the central layer thickness  $h_z$  decreases,

and the edge layer thickness  $h_b$  increases. In addition, the spreading radius  $r_t$  does not change considerably at  $t = 5.31$  ms, but the central layer thickness  $h_z$  falls and the edge layer thickness  $h_b$  grows, with the distinction between them reduced. There is no significant difference between  $t = 25.78$  ms and  $t = 5.31$  ms, indicating that the steady state has been attained. When compared to Figure 5, the oil layer thickness distribution is more stable throughout the spreading on the thin liquid film after impact, and no substantial retraction is observed.

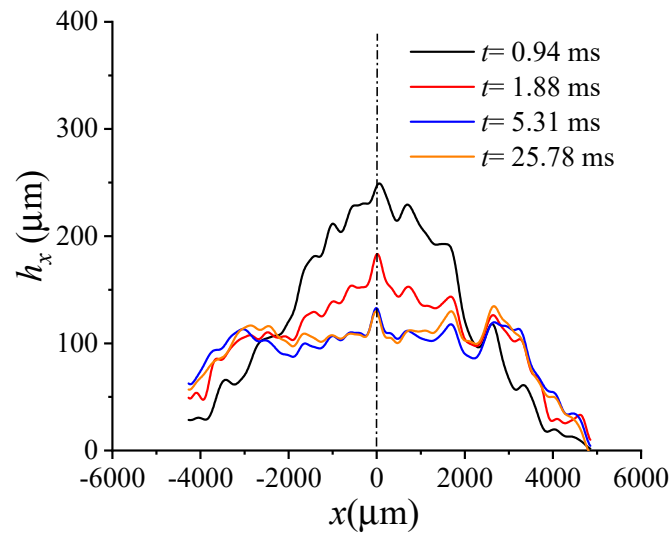


**Figure 12.** Distribution of oil layer thickness along the  $x$ -axis for PAO4 oil droplets impacting the sheet with ( $h_0 = 33 \mu\text{m}$ ,  $\delta = 0.011$ ) thin liquid film thickness at different moments ( $v = 2.73$  m/s,  $r_0 = 1.5$  mm).

Figure 13 illustrates the influence of thin liquid film thickness on the spreading behavior of PAO4 oil droplets. At the initial stage of impact ( $t = 0.94$  ms), the spreading patterns of oil droplets impacting the sheet with different thin liquid film thicknesses are similar; as time passes, the oil droplets impacting the sheet with different thin liquid film thicknesses have a more uniform distribution of oil thickness, a larger spreading radius; the edge layer thickness  $h_b$  is smaller, the retraction is weaker, and the central layer thickness  $h_z$  does not vary considerably. Figure 14 illustrates how the spreading of the different oil droplets is affected by thin liquid film thickness, and it can be seen that, the larger the viscosity, the more significant the influence of the thin liquid film.

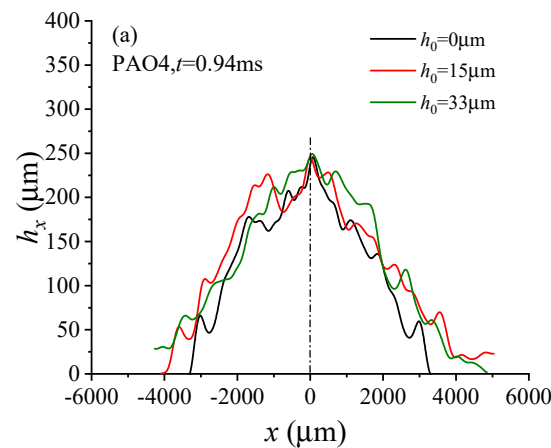


**Figure 13.** Cont.

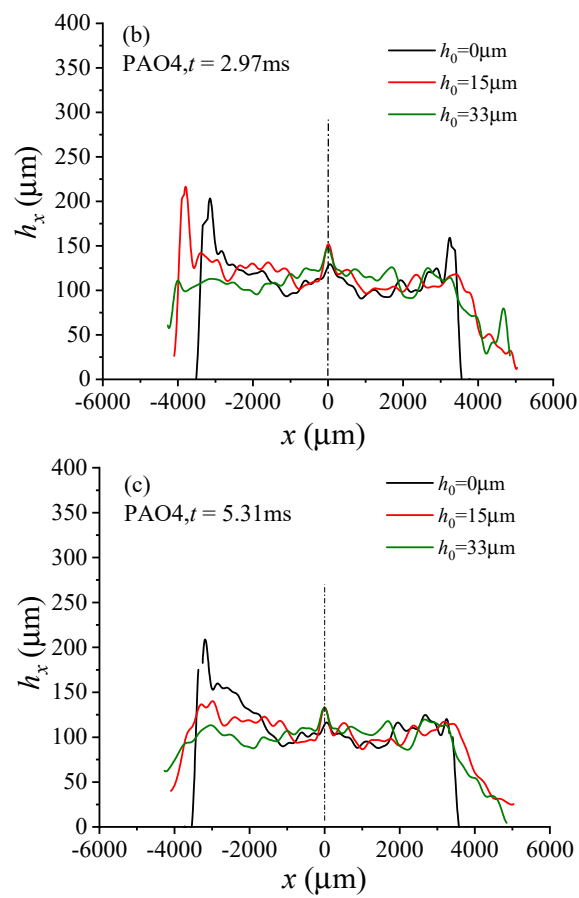


**Figure 13.** Comparison of the cross-sectional distribution of oil layer thickness at different thickness liquid film cross-sections by PAO4 oil droplet impacts: (a) PAO4,  $t = 0.94$  ms; (b) PAO4,  $t = 2.97$  ms; (c) PAO4,  $t = 5.31$  ms.

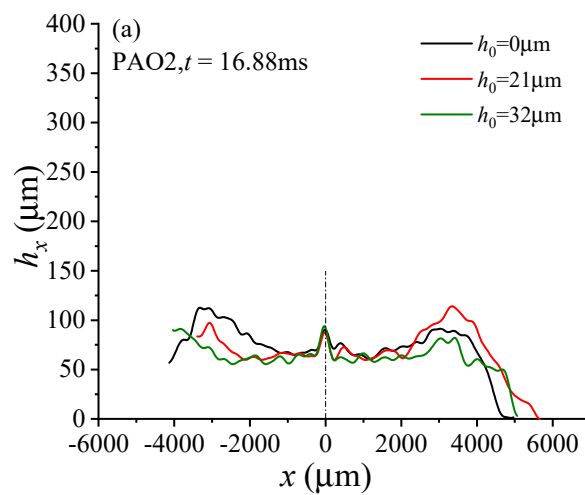


**Figure 14.** Cont.

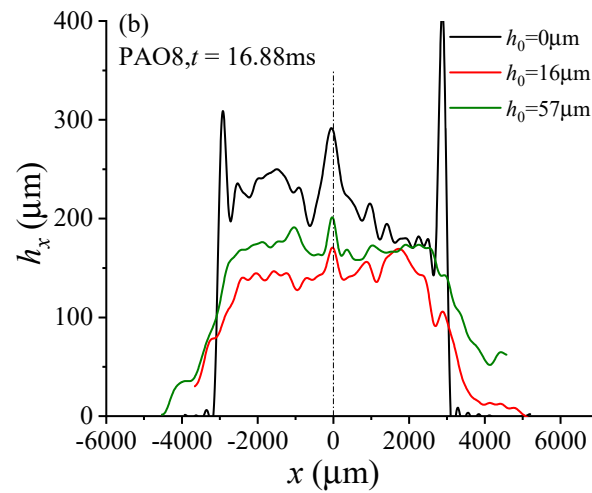


**Figure 14.** Comparison of the cross-sectional distribution of oil layer thickness for different oil droplets impacting the sheet with different thin liquid film thicknesses sections: (a) PAO2,  $t = 16.88$  ms; (b) PAO8,  $t = 16.88$  ms.

Figure 15 depicts the spreading factor changes against time when the PAO8 oil droplet impacted the sheet with different thin liquid film thicknesses. It can be seen that the spreading process may be divided into two stages. The first stage is from 0 to 2 ms, during which the thickness of the thin liquid film has little impact on the spreading radius. The second stage lasts from 2 to 100 ms; in this time, the droplet impacting the dry surface has already achieved the steady state, while the droplet impacting the sheet with thin liquid film goes on spreading: when the thin liquid film is 6  $\mu\text{m}$ , the droplet reaches the maximum spreading factor at  $t = 2$  ms and tends to be stable, and its spreading behavior is essentially the same with the change on the dry surface; when the thin liquid film is larger than 16  $\mu\text{m}$ , the spreading factor gradually increases, and the spreading factor increases as the thickness of the thin liquid film increases.

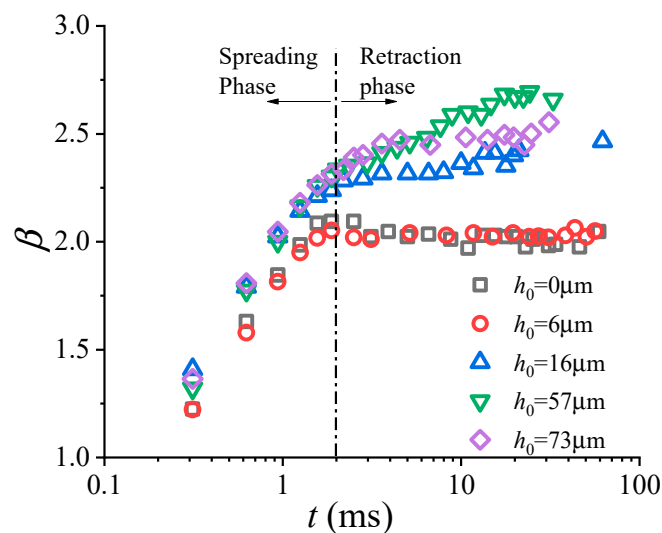


**Figure 15.** PAO8 oil droplet impacts the spreading factor over time for different thin liquid film thicknesses.

Figure 16 depicts the central layer thickness  $h_z$  curve against time for various oil droplets. The central layer thickness of PAO2 falls fast and then becomes stable. The thin liquid film has only a limited influence on the film thickness distribution of PAO2. The spreading of the PAO4 and PAO8 oil droplets can also be separated into two stages: the central layer thickness declines fast in the first stage, with less influence of the thin liquid

film; in the second stage, the central layer thickness grows and retraction occurs, and, the greater the thickness of the thin liquid film, the less noticeable the rise in central layer thickness, and hence, the less noticeable the retraction phenomena.

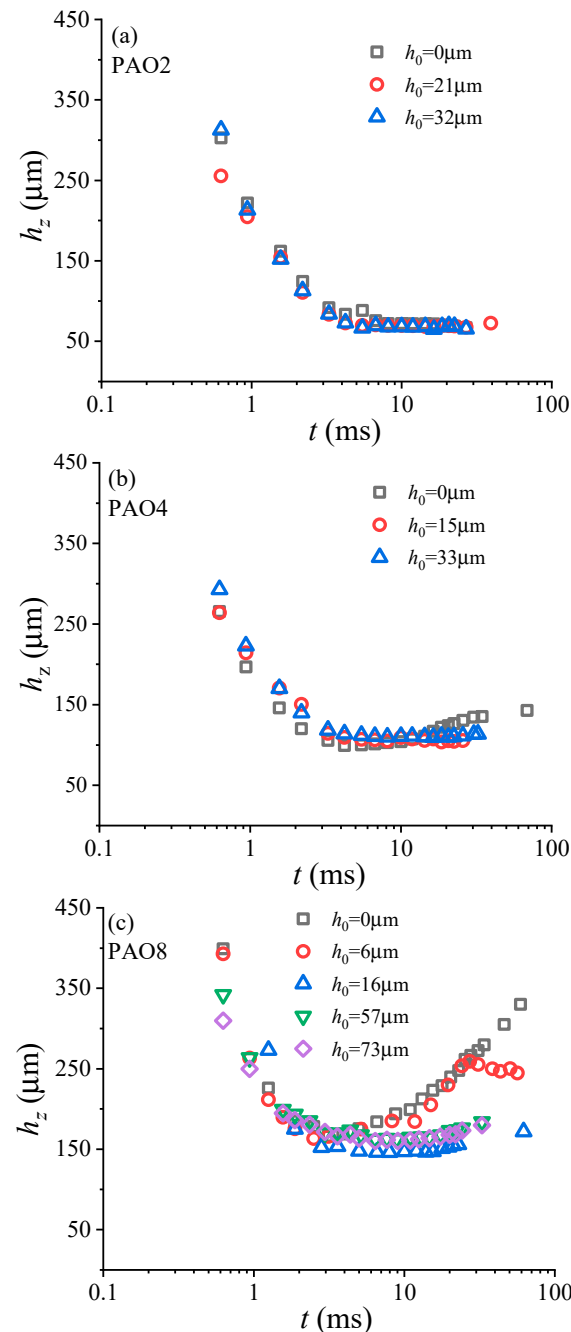


**Figure 16.** Central layer thickness as a function of time for different oil droplets impacting the sheet with different thin liquid film thicknesses: (a) PAO2; (b) PAO4; (c) PAO8.

#### 4. Discussion

In testing on a dry surface, the impact velocity is constant for all three oils, the contact angle difference is minor, and the latter effect is mostly caused by viscosity. As shown in Figures 7 and 8, in the impact phase from zero to two milliseconds the collapse of the oil droplets into thin oil layers is observed; a larger viscosity results in a smaller maximum spreading radius and thicker spreading oil layer. During the retraction phase (2 ms~100 ms), a larger viscosity leads to less splashing, a thicker central layer thickness, and dramatic retraction. In the testing with impacting thin liquid films, increasing the film

thickness has less effect on the spreading of PAO2 but a great effect on PAO8, indicating that the larger the viscosity, the more vulnerable it is to be influenced by a thin liquid film.

When comparing the results of PAO8 droplets impacting a dry surface and the thin liquid film, Figure 15 shows that the spreading central layer thickness on the thin liquid film 6  $\mu\text{m}$  thick is similar to that on the dry surface, whereas it changes on a thin liquid film more than 16  $\mu\text{m}$  thick. The thin liquid film has little effect on the spreading phase from zero to two milliseconds but has a significant effect on the retraction phase after two milliseconds. The spreading factor increases as the thickness of the thin liquid film grows (Figure 15), but the central layer thickness tends to vary gradually (Figure 16). Figure 17 depicts the spreading factor of PAO8 as well as the change in central layer thickness with liquid film thickness. Figure 17 shows the spreading factor of PAO8 and the change curve of central layer thickness with the thin liquid film thickness at  $t = 15$  ms. When the thin liquid film is less than 20  $\mu\text{m}$  thick, the spreading factor increases rapidly, and the central layer thickness increases rapidly in the steady state. When the thin liquid film is greater than 20  $\mu\text{m}$  thick, the spreading factor and central layer thickness change steadily with the thickness of the thin liquid film. This is essentially consistent with the change in stiffness of the thin liquid film: when the liquid layer thickness is in the order of microns, the stiffness of the thin liquid film will decrease with the increase in liquid film thickness. According to Yang's calculations and actual observations [21], when the liquid film thickness grows from 5 to 25  $\mu\text{m}$ , the stiffness of the thin liquid film rapidly drops from 900 N/m to 50 N/m under certain conditions.

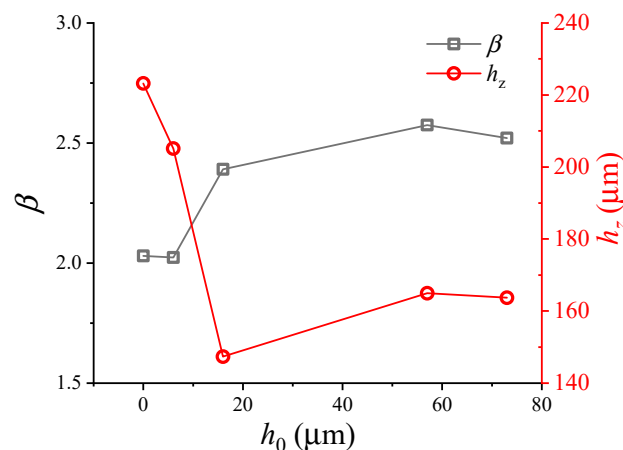


**Figure 17.** PAO8 spreading factor and variation of central layer thickness with a thin liquid film thickness at  $t = 15$  ms.

In terms of energy dissipation [22], the lower the stiffness, the more likely the thin liquid film is to distort. As a result, during the impact, not only the droplets but also the thin liquid film will be distorted, resulting in extra energy dissipation and a more uniform and steady spreading for the oil droplets.

## 5. Conclusions

The spreading behavior of oil droplets impacting a surface was observed from the frontal and the lateral view synchronously in this research, and the oil layer thickness distribution during spreading was determined using a laser-induced fluorescence technique. The spreading patterns of oil droplets impacting a dry surface and a surface covered with a thin liquid film were examined, and the effect of viscosity and thickness of the thin liquid film on the spreading radius and oil layer thickness distribution was studied. The results show that the larger the viscosity, the smaller the maximum spreading radius, the larger the thickness of the spreading center, and the greater the retraction. The effect of a thin liquid film on retraction is evident; a thicker thin film leads to a weaker retraction. In actuality, the surface cannot be completely dry; generally, it will be covered by a thin liquid film

from lubrication during operation. The test results will provide more accurate boundary conditions for the experimental and theoretical analysis of oil-air lubrication and shed some light on the development of oil-air lubrication theory.

1. The viscosity is a key factor affecting the pattern of impact and spreading when a single oil drop impacts a dry surface. A larger viscosity results in less splashing, a smaller maximum spreading factor, and a larger central layer thickness. The spreading of oil droplets with a higher viscosity after impacting can be significantly influenced by the presence of a thin liquid film on the surface.
2. During the spreading of the oil droplets, the spreading radius achieves its maximum and then remains almost stable, however, the thickness distribution of the oil layer continues to vary, with the central layer thickness increasing and the edge layer thickness decreasing, resulting in a retraction phenomenon. The greater the viscosity, the greater the retraction.
3. A thin liquid film of micrometer thickness can increase splashing while decreasing retraction. This is mostly due to a change in the stiffness of the thin liquid film.

**Author Contributions:** Investigation, formal analysis, writing—original draft preparation, P.Y.; Conceptualization, Writing—Review & Editing, H.L. and W.W.; Supervision, Project administration, Funding acquisition, H.L., W.W. and B.T.; Validation, Resources, Y.L. and X.G. All authors have read and agreed to the published version of the manuscript.

**Funding:** This research was funded by the National Natural Science Foundation of China (52175158, U2141243, 51975005).

**Data Availability Statement:** Not applicable.

**Conflicts of Interest:** The authors declare no conflict of interest.

## References

1. Shuyan, Z.; Feng, G.; Chao, L. Influence of Surface Wettability on Lubrication by Limited Lubricant Supply. *Tribology* **2017**, *37*, 429–434. [[CrossRef](#)]
2. Zhang, S.; Wang, W.; Li, X.; Guo, F. The Effect of Oil Droplet on the Lubrication Performance. *J. Tribol.* **2016**, *138*, 031506. [[CrossRef](#)]
3. Worthington, A.M., III. A Second Paper on the Forms Assumed by Drops of Liquids Falling Vertically on a Horizontal Plate. *Proc. R. Soc. Lond. Ser. A Math. Phys.* **1876**, *25*, 261–272.
4. Rioboo, R.; Marengo, M.; Tropea, C. Outcomes from a Drop Impact on Solid Surfaces. *At. Sprays* **2001**, *11*, 155–166. [[CrossRef](#)]
5. Rioboo, R.; Marengo, M.; Tropea, C. Time evolution of liquid drop impact onto solid, dry surfaces. *Exp. Fluids* **2002**, *33*, 112–124. [[CrossRef](#)]
6. Fei-Fei, B.; Ya-Li, G.; Sheng-Qiang, S.; Jue-Xian, C.; Yi-Qiao, L. Experimental study of spread characteristics of droplet impacting solid surface. *Acta Phys. Sin.* **2012**, *61*, 293–298. [[CrossRef](#)]
7. Hong, L.; Shu-chun, W.; Mao-zhao, X.; Ming, J.; Jun-rui, S.; Yu-feng, S. Numerical Simulation of Secondary Atomization on Impacting of a Droplet upon a Thin Liquid Film. *J. Combust. Sci. Technol.* **2012**, *18*, 38–43.
8. Motzkus, C.; Gensdarmes, F.; Géhin, E. Parameter study of microdroplet formation by impact of millimetre-size droplets onto a liquid film. *J. Aerosol Sci.* **2009**, *40*, 680–692. [[CrossRef](#)]
9. Gang-tao, L. Study of Drop Impact Dynamics on Liquid Film. Ph.D. Thesis, Dalian University of Technology, Dalian, China, 2014.
10. Wang, A.B.; Chen, C.C. Splashing impact of a single drop onto very thin liquid films. *Phys. Fluids* **2000**, *12*, 2155–2158. [[CrossRef](#)]
11. Vander Wal, R.L.; Berger, G.M.; Mozes, S.D. Droplets splashing upon films of the same fluid of various depths. *Exp. Fluids* **2006**, *40*, 33–52. [[CrossRef](#)]
12. Ghielmetti, C.; Marengo, M.; Mundo, C.; Tropea, C. Experimental Investigation of a Polydispersed Water Spray Impinging on a Conical Surface. *Int. J. Fluid Mech. Res.* **1997**, *24*, 358–369. [[CrossRef](#)]
13. Walzel, P. Zerteilgrenze beim Tropfenprall. *Chem. Ing. Tech.* **1980**, *52*, 338–339. [[CrossRef](#)]
14. Prosperetti, A.; Oguz, H.N. The Impact of Drops on Liquid Surfaces and the Underwater Noise of Rain. *Annu. Rev. Fluid Mech.* **2003**, *25*, 577–602. [[CrossRef](#)]
15. Rein, M. Phenomena of liquid drop impact on solid and liquid surfaces. *Fluid Dyn. Res.* **1993**, *12*, 61–93.
16. Wu, M.; Wei, W.; Yuan, S.; Hu, J. Study of Multiple-Point Oil- Jet Lubrication of High-Speed Ball Bearings. *Power Transm. Eng.* **2014**, *6*, 44–46.
17. Hidrovo, C.H.; Hart, D.P. Emission reabsorption laser induced fluorescence (ERLIF) film thickness measurement. *Meas. Sci. Technol.* **2001**, *12*, 467. [[CrossRef](#)]

18. Zhou, S.Q.; Ni, R.; Funfschilling, D. Effects of shear rate and temperature on viscosity of alumina polyalphaolefins nanofluids. *J. Appl. Phys.* **2010**, *107*, 219. [[CrossRef](#)]
19. Zheng, N.; Tong, B.; Zhang, B.; Hu, A.; Liang, H.; Wang, W.; Liu, D. Numerical study on flow and heat transfer characteristics of two oil droplets impinging the wall simultaneously under the influence of micro-bubble. *Int. J. Heat Mass Transf.* **2022**, *190*, 122793.
20. Chen, L.; Bonaccorso, E.; Deng, P.; Zhang, H. Droplet impact on soft viscoelastic surfaces. *Phys. Rev. E* **2016**, *94*, 063117. [[CrossRef](#)] [[PubMed](#)]
21. Wen-jing, Y. Study on Dynamic Characteristics of Liquid Film Seal Based on Cavitation Effect. Ph.D. Thesis, China University of Petroleum (East China), Dongying, China, 2019.
22. Howland, C.J.; Antkowiak, A.; Castrejón-Pita, J.; Howison, S.D.; Oliver, J.M.; Style, R.W.; Castrejón-Pita, A. It's Harder to Splash on Soft Solids. *Phys. Rev. Lett.* **2016**, *117*, 184502. [[CrossRef](#)] [[PubMed](#)]

**Disclaimer/Publisher's Note:** The statements, opinions and data contained in all publications are solely those of the individual author(s) and contributor(s) and not of MDPI and/or the editor(s). MDPI and/or the editor(s) disclaim responsibility for any injury to people or property resulting from any ideas, methods, instructions or products referred to in the content.